Ma, F., Swainsbury, D. J. K., Jones, M. R., & van Grondelle, R. (2017). Photoprotection through ultrafast charge recombination in photochemical reaction centres under oxidizing conditions. *Philosophical Transactions B: Biological Sciences*, *372*(1730), [20160378]. https://doi.org/10.1098/rstb.2016.0378

Photoprotection through ultrafast charge recombination in photochemical reaction centers under oxidizing conditions

Fei Ma[1,*], David J. K. Swainsbury[2,3], Michael R. Jones[2] and Rienk van Grondelle[1]

[1]Department of Biophysics, Faculty of Sciences, VU University Amsterdam, De Boelelaan 1081, 1081 HV Amsterdam, The Netherlands
[2]School of Biochemistry, University of Bristol, Medical Sciences Building, University Walk, Bristol BS8 1TD, United Kingdom
[3]Present address: Department of Molecular Biology and Biotechnology, University of Sheffield, Sheffield S10 2TN, United Kingdom

Key words
reaction center, photoprotection, charge recombination, ultrafast spectroscopy, styrene maleic acid

Abstract

Engineering natural photosynthesis to address predicted shortfalls in food and energy supply requires a detailed understanding of its molecular basis and the intrinsic photoprotective mechanisms that operate under fluctuating environmental conditions. Long-lived triplet or singlet excited electronic states have the potential to cause photodamage, particularly in the presence of oxygen, and so a variety of mechanisms exist to prevent formation of such states or safely dissipate their energy. Here we report a dramatic difference in spectral evolution in fully reduced and partially oxidized *Rhodobacter sphaeroides* reaction centers (RCs) following excitation of the monomeric bacteriochlorophyll (BChl) cofactors at 805 nm. Three types of preparation were studied, including RCs purified as protein/lipid nanodiscs using the copolymer styrene maleic acid. In fully reduced RCs such excitation produces membrane-spanning charge separation. In preparations of partially oxidized RCs the spectroscopic signature of this charge separation is replaced by that of an energy dissipation process, including in the majority sub-population of reduced RCs. This process, which appears to take place on both cofactor branches, involves formation of a $BChl^{+}$/bacteriopheophytin^{-} radical pair that dissipates energy via recombination to a vibrationally hot ground state. The possible physiological role of this dissipative process under mildly oxidizing conditions is considered.

1. Introduction

Concerns over meeting mankind's projected increased demands for food and sustainable energy resulting from growth of the global population and increased levels of development are fuelling research into strategies for enhancing natural photosynthesis and developing novel ways of harvesting solar energy [1−3]. Although it provides the principal means of powering the biosphere, natural photosynthesis is a relatively inefficient process in which only a few percent of the energy of absorbed photons is converted into biomass [4−6]. There is therefore optimism that the energy efficiency of natural photosynthesis can be enhanced to produce higher yielding crops [2,7,8].

Concerted application of spectroscopy, structural biology and genetic modification has revealed many of the molecular details of the first steps of the photosynthetic process in which solar energy is harvested and converted into chemical energy [9,10]. Alongside the evolution of biomolecular structures and mechanisms for this solar energy conversion a set of protective mechanisms have evolved to prevent damage when flows of energy and electrons through photosystems are not optimal. In principle these photoprotective mechanisms could directly impact on the mechanism for energy conversion. An example is the idea that free energy of states involved in light powered electron transfer is tuned not only to promote efficient electron transfer but also to avoid unwanted sensitization of singlet oxygen [11].

Reaction centre (RC) pigment-proteins facilitate the key reaction of photosynthesis in which harvested solar energy is used to separate electrical charge across a lipid bilayer membrane [12−14]. The important steps in this process occupy time regimes from a fewpicoseconds for light harvesting and primary charge separation through to a few milliseconds for the diffusional processes that remove electrons from the RC and deliver replacements. As conditions that slow quenching of singlet excited state energy by RCs can lead to formation of long-lived (bacterio)chlorophyll triplet excited states, sensitization of singlet oxygen and photodamage, a variety of mechanisms have evolved for photoprotection through dissipation of excess or long-lived excited states [15−17].

Much of our understanding of fundamental aspects of biological solar energy conversion and photoprotection has come from studies of the RC from *Rhodobacter* (*Rba.*) *sphaeroides* [12,13,14,18,19]. As outlined in figures S1 and S2, picosecond

time scale charge separation in this protein occurs between a pair of bacteriochlorophyll (BChl) *a* molecules in their singlet excited state (P*) and a quinone (Q_A) via a monomeric BChl (B_A) and a bacteriopheophytin *a* (BPhe - H_A). After completion of the reaction scheme $P^*\rightarrow P^+B_A^-\rightarrow P^+H_A^-\rightarrow P^+Q_A^-$, P^+ is re-reduced by a molecule of cytochrome (cyt) c_2 (figure S1) on a timescale of microseconds to milliseconds [20]. As ~200 ps charge separation to form $P^+Q_A^-$ is much more rapid than reduction of P^+ by cyt c_2, P is expected to spend significant periods in the photo-oxidized state. Such RCs are described as being "closed" and, in principle, this circumstance could result in the formation of triplet excited states and photodamage. However a remarkable feature of purple bacterial photosystems is that closed RCs accept energy from the LH1 antenna with a lifetime of around 200 ps, only four-fold slower than in the case for "open" RCs with P reduced [21,22]. This implies a mechanism whereby P^+ can accept energy from other pigments.

Insights into the possible mechanism of energy quenching by P^+ have largely come from experiments in which B or H is excited. It has been observed that directly formed B* (a mixture of B_A* and B_B*) has a lifetime of 100~250 fs irrespective of whether P is reduced or oxidized [23−29]. A variety of mechanisms for energy or electron transfer from B* to P^+ have been suggested (see Discussion section), but quenching of excited state energy by closed RCs is not fully understood.

The initial aim of this work was to compare the process of charge-separation in a novel RC-polymer preparation with that in RCs native membranes or detergent micelles. The polymer, styrene maleic acid (SMA), solubilizes RCs from the native membrane along with ~150 lipids as a polymer/lipid/protein nanodisc [30]. On investigating "as-prepared" RC-SMA nanodiscs and native membranes, which displayed partial oxidation of P (figure S3B), a remarkable change in ultrafast spectral response was obtained following excitation of B_A/B_B at 805 nm. We conclude that a mechanism operates in open RCs exposed to a moderately oxidizing ambient potential that dissipates energy entering the RC through either B or connected pigments. Our findings provide new insights into how RCs are protected against fluctuating environmental conditions and assign a new photoprotective role to the BChl and, in particular, the specialist H cofactor that make up the so-called "inactive branch" of RC cofactors.

2. Results

(a) Comparison of charge separation in three types of reduced RC

Transient absorbance difference spectra were recorded in the presence of sodium ascorbate to achieve a uniform population of P-reduced RCs (figures S3A and S4). Analysis of *n*-dodecyl *β*-D-maltoside (DDM)-purified, SMA-purified and membrane-embedded (MEM) RCs focused on the Q_y absorbance bands (figure S3A) at 760 nm (H_A/H_B), 802 nm (B_A/B_B) and 865 nm (P); time resolved absorbance difference spectra are shown in figure S4. Following direct excitation of P at 870 nm, P* stimulated emission (SE) at 915 nm (figure 1A, circles) decayed with a time constant of 3.9 ps (DDM), 4.2 ps (SMA) and 4.3 ps (MEM) (error ±0.2 ps). At 755 nm (figure 1A, triangles) decay of BChl *a* excited state absorbance (ESA) [31] and growth of H ground state bleaching (GSB) were concerted. The latter had a recovery time of ~200 ps, attributable to charge transfer from $P^+H_A^-$ to $P^+Q_A^-$.

For ascorbate-reduced RCs spectra were also recorded following non-selective excitation of B at 805 nm (figure S5). B* decayed with a time constant of 230 fs (DDM), 220 fs (SMA) and 200 fs (MEM) (figure 1B, 805 nm traces), in line with published values [29]. Previous work from our laboratories [31−33] has established that this decay is due to parallel B*→P energy transfer, B_A*→$P^+B_A^-$ and B_A*→$B_A^+H_A^-$ charge separations (see figure S2). P* was formed with the same time constants as decay of B*, and in turn decayed with a time constant of 3.9 ps (DDM), 4.2 ps (SMA) and 4.2 ps (MEM) (figure 1B, 915 nm traces, errors ± 0.2ps). Kinetic traces at 755 nm (figure 1B, triangles) showed a ~200 fs component attributable to the decay of B ESA, a ~4 ps component attributable to P* to $P^+H_A^-$ conversion and a ~200 ps component arising from $P^+H_A^-$ to $P^+Q_A^-$ conversion. The conclusion from this analysis was that, as determined previously for membrane-bound RCs [34], initial charge separation in SMA-purified RCs was somewhat slower than in RCs in detergent solution.

(b) Charge separation in partially oxidized RCs following excitation of P or B

During purification, the exposure of membranes and RCs to buffers containing dissolved oxygen can result in partial oxidation of P, producing a partial bleaching of the 865 nm band (figure S3B). The extent of oxidization $\emptyset_{ox} = \frac{[ox]}{[ox]+[red]}$ is

determined by $(10^{\frac{\epsilon^0-\epsilon}{59.2}}+1)^{-1}$, where ϵ is P/P^+ redox potential of the as-prepared RC and ϵ^0 is the respective mid-point redox potential. ϵ and ϵ^0 are obtained from electrochemistry measurements, by fitting the dependence of $\frac{P}{B}$ absorption band ratio on applied electric potential [30]. Values of ϵ^0 for the SMA-purified (443 mV) and membrane-embedded (449 mV) RCs are lower than for DDM-purified RCs (465 mV). Yet the membrane-embedded (ϵ=435 mV, $\emptyset_{ox}$ = 0.39) and SMA-purified (406 mV, 0.19) RCs are more sensitive to the ambient oxygen, and more P molecules are oxidized than that in the DDM-purified RC (375 mV, 0.03). The three "as prepared" RC samples as a result constitute a system suitable for quantitatively investigating the effect of redox state of P on the charge separation and transfer dynamics.

In transient absorbance spectra of "as prepared" RCs excited at 870 nm (figure S6) P* decayed with time constants of 4.0 ps (DDM), 7.1 ps (SMA) and 12.7 ps (MEM) –see kinetic traces at 915 nm in figure 2 (circles). Hence partial oxidation of P was associated with a marked slowing of P* decay. Using the extent of H-band GSB between 100 and 1000 ps as a guide it was also apparent that less H_A^- was formed when P was partially oxidized (compare the red and black 755 nm traces in figure 2). Origins of these effects are considered in the Discussion section.

For "as-prepared" DDM-purified RCs, which displayed very little P oxidation, the measured spectral evolution after 805 nm excitation (figure 3A) was similar to that obtained with ascorbate-reduced DDM RCs (figure S5A), with lifetimes of 220 fs for B* and 4.1 ps for P*. However absorbance difference spectra recorded for the "as-prepared" membrane-embedded (figure 3B) and SMA-purified (figure S7) RCs showed dramatic changes compared to the equivalent spectrum for ascorbate-reduced RCs (figure S5B,C) and both types of DDM RC (figures 3A and S5A). The most obvious of these was a near complete loss of P-band GSB, implying a very strong reduction in the yield of P* and/or P^+ (compare figures 3A and 3B).

For "as-prepared" membrane-embedded RCs, 805 nm excitation produced an immediate B-band GSB and BChl ESA below 760 nm (figure 3B, 0.1 ps trace). Unusually weak P-band GSB and P* SE, attributable to some B*→P energy transfer, reached a maximum at ~150 fs (0.1 ps trace in inset to figure 3B). Then, in marked contrast to the equivalent data obtained with ascorbate-reduced RCs (figure S5C) and "as-prepared" DDM RCs (figure 3A), the weak negative band between 830 and 930 nm decayed rapidly and a broad, weak absorbance band centered at 880 nm formed

with a time constant of 220 fs (see insets to figure 3B). This new absorbance band, to our knowledge, has not been reported previously and here we refer to the corresponding state as A1. This band reached a maximum at ~0.8 ps and then decayed with a time constant of 4.5 ps (see lower inset in figure 3B). Simultaneous with this decay a second absorbance band developed with a maximum at 815 nm, which we refer to as belonging to a second state A2. The superposition of the A1 and/or A2 absorbance caused a splitting of the large negative band between 770 and 800 nm attributable to B-band GSB. After the A1 state had decayed to zero (20 ps trace in figure 3B), the difference spectrum of the A2 state comprised two derivative-shaped bands at ~800/815 nm and ~755/770 nm (negative/positive). The A2 state reached a maximum after 4.5 ps and then decayed with a time constant of 10.2 ps, after which only a very small component remained that was attributable to a very low level of $P^+H_A^-$.

Consideration of kinetic traces (figure 4) revealed a correlation between the decay of A1 and formation of A2, suggesting a direct A1→A2 transition. In the B-band at 795 nm there were three recovery time constants (figure 4, black). The 200 fs component corresponded to the lifetime of B*, and was comparable to that obtained with the equivalent reduced RC. The next 4.5 ps component corresponded to the decay of the A1 state. Final recovery of B-band GSB occurred with the same time constant (10.2 ps) as the A2 lifetime (see above), implying that A2 is a state that involves one or both B molecules.

The 880 nm kinetic trace (figure 4, blue) had two components of 220 fs (−) and 4.5 ps (+). The development of the negative signal, reflecting fast B*→P energy transfer, was expected to have an equivalent time constant to the lifetime of B* (200 fs). However, it reached a maximum at 130 fs due to mixing with the growth of A1 absorbance. The early kinetics were dominated by a 220 fs decay of P-band GSB, and as this ultrafast decay of the spectroscopic signature of P* was not observed in reduced RCs, and it was not seen when P was excited directly, it was most likely associated with overlapping spectral changes arising from formation of the A1 state. Having formed with a lifetime of 220 fs, the A1 absorbance decayed with a lifetime of 4.5 ps (figure 4, inset, blue). After 50 ps only a very small negative component was present due to $P^+Q_A^-$. Its relative amplitude was only 0.016 compared to the maximal negative ΔA value at 40 fs.

The 820 nm kinetic trace (figure 4, red) contained contributions from B-band

GSB and the subsequent absorbance of both the A1 and A2 states. It had three components of 200 fs (−), 3.7 ps (−) and 10.2 ps (+), corresponding to the lifetime of B*, the time constant of the A1→A2 transition and the lifetime of A2, respectively. The 755 nm kinetic trace (figure 4, green) contained contributions from the ESA of BChl *a* and H-band GSB. It had three components of 200 fs (+), 4.5 ps (−) and 10.5 ps (−), corresponding to the lifetime of B*, and the bi-exponential recovery of the H-band GSB, respectively. The H-band GSB formed with a 200 fs time constant, as opposed to the 4-12 ps time constant seen for reduced RCs or RCs excited at 870 nm. Thus H^- was formed directly following photoexcitation rather than through the process $P^*\rightarrow P^+B^-\rightarrow P^+H^-$. The synchronous nature of the decays of B-band and H-band GSB indicated that A1 and A2 are states that contain contributions from both B and H.

"As-prepared" SMA-purified RCs exhibited a similar spectral evolution with similar time constants (see figure S7), although the spectral shapes were a little different. In particular this applied to the negative signal corresponding to P*, the shape of the A1 absorbance and the negative signal in the B band region before 1 ps. This is likely due to the presence of more reduced RCs in the sample of SMA-purified RCs (0.81) than in that of membrane-embedded RCs (0.61), and slight differences in the electronic structures of the excited states in different environments. In the 880 nm kinetic trace for SMA RCs (figure S8) the ratio of the amplitude of the long-lived GSB to the maximal negative ΔA was 0.064, four times larger than the value of 0.016 obtained for membrane-embedded RCs, implying a somewhat greater formation of $P^+Q_A^-$. The characteristic time constants for the SMA RCs were 240 fs, 4.2 ps and 9.7 ps, corresponding to the lifetimes of B*, A1 and A2, respectively.

Absorbance signals of both A1 and A2 were linearly dependent on the excitation intensity (figure S9) and were not dependent on the sample concentration over an OD_{805} range from 0.2 to 1.2 with an excitation intensity of 100 nJ/pulse. The time-evolution of the A1 and A2 states was therefore not influenced by any nonlinear processes. In addition, absorbance spectra recorded before and after data acquisition showed that there was no change in the overall redox state of the "as prepared" SMA and MEM RCs during measurements. It was also possible to rule out that the A1 and A2 states arose as a result of photo-accumulation of a state such as P^+Q^- during the ultrafast measurements, and such a state would also be expected to be formed in the "as-prepared" DDM RCs.

The long-lived P GSB signal at 865 nm representing formed P^+Q^- reflects how much physiological function remains, i.e., how much effective charge separation and transfer occurs. The ΔA values of the as-prepared RCs compared to that of the ascorbate-reduced RCs, θ, are 0.92, 0.15 and 0.04 for the DDM, SMA and MEM RCs, respectively. Their dependence on the extent of oxidization $\emptyset_{ox}$ (including two limit situations that θ=1 for totally reduced RC and θ=0 for totally oxidized RC) is fitted with an exponential function (figure S10). It shows that θ decreases to e^{-1} when $\emptyset_{ox}$ is 0.12.

3. Discussion

(a) SMA/lipid nanodiscs preserve a membrane environment for charge separation.

Previous work has shown that the kinetics of charge separation are subtly sensitive to the environment of the *Rba. sphaeroides* RC [34], the lifetime of P* being longer for membrane-embedded RCs (4.5 ps) than for RCs purified using the detergent lauryldimethylamine oxide (3.3 ps). The P* lifetime of 4.2 ps determined above for RCs in SMA/lipid nanodiscs was similar to the 4.2-4.3 ps for RCs in native membranes and slower than the 3.9 ps obtained for DDM RCs, reinforcing a recent conclusion that these nanodiscs preserve a membrane-like environment for the RC [30]. In addition these nanodiscs present some distinct experimental advantages over native membranes as the RC protein can be prepared in a pure and highly concentrated form, with the same scattering and viscosity characteristics as RCs in detergent solution.

During RC purification it is not unusual to observe a partial oxidation of P. To our surprise, "as prepared" membrane-embedded and SMA-purified RCs showed a substantial loss of P*-driven charge separation after excitation at 805 nm, in contrast to "as-prepared" DDM RCs and all samples with added ascorbate. Instead of obtaining strong negative signals between 830 and 930 nm characteristic of formation of P* and P^+ in the major P-reduced sub-population, positive signals developed within 1 ps indicating fast dissipation of the energy of B* through a route involving the two states we label A1 and A2.

(b) Evolution associated difference spectra (EADS) to identify the A1 and A2

states.

EADS of the states formed after 805 nm excitation of "as prepared" SMA and MEM RCs obtained by global analysis are shown in figure 5. The EADS with a 150 fs lifetime is attributable to B*, and that with a 220 fs lifetime to a complex mix of GSB and ESA of the B-band, a contribution of A1 (splitting of the negative band at 815 nm), and some P-band GSB with P* SE. The next EADS, attributable to A1 (figure 5, red – lifetime 4.5 ps), had a broad absorbance at 880 nm and GSB in both B- and H-band. As absorbance difference spectra of both ΔBChl$^+$ *a* (i.e. BChl$^+$ *a*−BChl *a*) and ΔBPhe$^-$ *a* (i.e. BPhe$^-$ *a*–BPhe *a*) have a maximal absorbance at ~880 nm [26,36], the simplest attribution of A1 is a B^+H^- charge-transfer (CT) state which develops from B* with a lifetime of 200 fs and decays to A2 with a lifetime of 4.5 ps.

The EADS of state A2 was characterized by derivative-shaped features in both the B and H spectral regions (figure 5, blue – lifetime 10 ps). A derivative line shape is typical of the difference spectrum of a hot ground state, and the 10 ps lifetime is in the range of a few ps to several tens of ps that is typical of the cooling time of a hot ground state [37]. We therefore attribute A2 to a hot ground state, $(BH)^{hot}$, that is formed by charge recombination from B^+H^- with a lifetime of 4.5 ps and decays by vibrational relaxation with a lifetime of 10 ps. Formation of a hot ground state of B_B was proposed in a recent report on quenching of B_A* and B_B* states in fully oxidized RCs, but the participation of H in the process leading to this was not suggested [38]. Instead, it was proposed that the reaction sequence $P^+B_B^* \rightarrow P'B_B^+ \rightarrow P^+B_B^{hot} \rightarrow P^+B_B$ occurs in oxidized RCs, where P' is an unrelaxed P neutral state formed by electron transfer from B_B* to P^+. This process was suggested to take place alongside energy transfer to P^+ from either B_A* or B_B* to form P^+*, although no spectroscopic evidence for formation or decay of such an excited state cation was obtained [38]. This proposed $P^+B_B^{hot}$ state had a similar derivative spectral shape and decay time constant as A2. However, in the present data we find that GSB of both H and B recover with the decay of A2 and there is no signal corresponding to P^+, indicating that both H and B are involved in the A2 state but P^+ is not. In other studies it has also been suggested that the reaction sequences $P^+B^* \rightarrow PB^+ \rightarrow P^+B$ or $P^+B^* \rightarrow P^*B^+ \rightarrow P^+B$ (or P^+*B) could account for rapid quenching of B* by P^+ [27], and possible P^+ transitions that could facilitate energy transfer from B* have been explored [39]. Although, for the present work, any of these processes could account for B* quenching in the sub-population of

SMA or MEM RCs in which P is oxidized, they cannot account for B* quenching in the majority fraction where P is reduced, as such energy transfer from B* would simply form P*. The lack of a strong GSB of P shows that this process does not happen.

A_2 intermediating the B^+H^- CT and the ground states may have another origin in addition to hot ground state: triplet B^+H^- CT state. This possibility is inspired by the fact that in some conjugated polymers and organic compounds singlet-triplet splitting of CT state is small [40−43]. Further, 10 ps is also in the lifetime range of triplet CT states [43]. As a result, unambiguous assignment of A2 still need further work.

(c) Photochemical charge separation is dramatically altered under oxidizing conditions.

As far as we are aware, the finding that partial oxidation of P leads to a drastically reduced yield of the process $P^*\rightarrow P^+H_A^-$ when the initial excited state formed is B* has not been reported previously, nor has the finding that partial oxidation of P produces a slowing of $P^*\rightarrow P^+H_A^-$ in the remaining reduced RCs following direct excitation of P at 870 nm (figure 2). The likely reason is that ultrafast processes are easier to study in a uniform sample and partial P oxidation can easily be corrected with mild reductants. Previous studies of dynamics in oxidized RCs have employed high concentrations (5-500 mM) of potassium ferricyanide to oxidize P [25−29] or used a high excitation rate to photoaccumulate P^+ [38], whereas studies of excitation trapping in closed RC-LH1 complexes have used a high excitation intensity and/or background illumination to photo-accumulate P^+ [21,22].

The slowed P*-driven charge separationin partially oxidized RCs is induced by a removing of the $P^*\rightarrow P^+$ transition equilibration away from P^+, which is the result of a decreased $[P]/[P^+]$. In other words, the overall $P^*\rightarrow P^+$ activation energy of the sample (ΔG) increases. The effect of partial oxidation is therefore similar to that of mutations that raise the P/P^+ potential, such as the heavily studied P hydrogen bond mutations [44,45], where making P harder to oxidize and slows charge separation by increasing the activation energy for the reaction.

As a result of the movement of $P^*\rightarrow P^+$ equilibration, the spectral evolution of partially oxidized sample following B* was dominated by the A1 state which we attribute to B^+H^-, formed with a lifetime of ~200 fs. Unraveling the dynamic

processes that lead to the formation of B^+H^- under these conditions is difficult, as the time constants for formation of B^+, H^- and P* are all the same as the lifetime of B*, and the spectroscopic signatures of B^+ and H^- overlap with those of P*. In the case of P-oxidized RCs it is simple to postulate that initially-formed P^+B^*H relaxes to $P^+B^+H^-$ on the time scale of a few hundred femtoseconds (Mechanism 1 in Scheme 1).

The reason why, in the major fraction of P-reduced SMA and MEM RCs, direct formation of B* does not simply result in energy transfer to P (Mechanism 3 in Scheme 1) is also the result of the movement of equilibration. Previous studies of B* decay in fully reduced RCs [31−33,46] have revealed two P*-independent two-step routes for charge separation that connect B* to P^+H^-, namely $B^*\rightarrow P^+B^-\rightarrow P^+H^-$ and $B^*\rightarrow B^+H^-\rightarrow P^+H^-$ (Mechanisms 4 and 6, respectively, in Scheme 1). They also appear in the fully reduced DDM, SAM and membrane RC samples (the proof can be seen in figure S3 and S4, where appearance of the H GSB is much earlier when B is excited than P is excited). These two processes take place on a similar time scale to B*→P energy transfer (Mechanism 5), and the evolution of the system after B band excitation therefore depends on the precise rates of the three parallel processes under the particular experimental conditions (see legend to figure S2). $[P]/[P^+]$ determines the equilibration of the whole system, and thus tunes the branching ratios of the three parallel processes.

Given this, a simple explanation could be that the routes of B* decay via states requiring P/P^+ and P^*/P^+ redox changes are less favorable than is the case in fully reduced RCs, and so the only unaffected initial process, $B^*\rightarrow B^+H^-$, dominates (Mechanism 2 in Scheme 1). In fully-reduced RCs any formation of PB^+H^- would then be expected to relax via hole transfer to form P^+BH^- (as in Mechanism 4), but in partially-oxidized RCs destabilization of P^+ formation may make this uncompetitive compared with 4.5 ps recombination of B^+H^- to form $(BH)^{hot}$. As a result Mechanism 2 is followed and excitation of B leads to energy dissipation via B^+H^- and $P(BH)^{hot}$ even though P is not oxidized.

(d) Is a BPhe at the H_B site present to facilitate photoprotection?

To this point reference has been made to B^+H^- and $(BH)^{hot}$ states without attempting to distinguish between processes affecting B_A/H_A or B_B/H_B, but 805 nm excitation (FWHM 10 nm) is not selective for formation of B_A* or B_B*. Our data

suggests that the process $B^*H \rightarrow B^+H^- \rightarrow (BH)^{hot} \rightarrow BH$ can occur on either cofactor branch. This would be logical if this energy dissipation mechanism has a photoprotective function, as there is presumably an equal chance of excited state energy entering a RC via B_B/H_B or B_A/H_A. Intriguingly, a photoprotective mechanism operating under oxidizing conditions whereby the energy of a B_B^* (or H_B^*) excited state can be dissipated through formation and recombination of $B_B^+H_B^-$ would provide a reason for a specialized BPhe cofactor being present at the H_B site on the "inactive branch".

(e) Physiological relevance

Rba. sphaeroides is a metabolically-diverse photosynthetic organism that is able to grow in the dark through a variety of forms of anaerobic and aerobic respiration. To achieve photosynthetic growth the organism interfaces its light harvesting proteins and RCs with additional components, ubiquinone, cyt c_2 and the cyt bc_1 complex which also participate in aerobic respiratory electron transfer. Such component sharing between electron transfer chains presents challenges, and for example it has been shown that photosynthetic electron transfer is blocked in the presence of overly-reducing carbon sources, but can be reactivated through the addition of oxygen or alternative electron acceptors to restore a suitable redox poise to the intramembrane ubiquinone pool [47,48]. As *Rba. sphaeroides* is found in a variety of soil and freshwater habitats that are likely to experience fluctuations in electron donors and acceptors, including oxygen, efficient and non-destructive operation of its photosynthetic electron transfer chain has to be able to tolerate conditions where RCs are closed through over-reduction at the acceptor (ubiquinone/ubiquinol) interface or over-oxidation at the donor (P/cyt c_2) interface.

In this report we describe a new mechanism which serves to dissipate energy in RCs in which P is reduced, but ambient conditions are sufficiently oxidizing that other RCs in the population are closed through formation of P^+. We speculate that this mechanism is activated as the mean free energies of states involving P^+ rise in still-open RCs due to partial closure of the RC population under oxidizing ambient conditions. In RCs where P is excited directly the decay of P* is slowed, and in RCs where B is directly excited P* formation is lost and instead ultrafast formation of a B^+H^- radical pair dissipates energy through a two-step recombination to the ground state. Such a mechanism could contribute to the disfavoring of triplet state formation

under conditions where the balance of the cyclic photosynthetic electron transfer chain is disturbed due to overly-oxidizing conditions. This photoprotective mechanism has not been reported previously and provides a reason for retention of a specialized BPhe in the so-called inactive cofactor branch.

Data Accessibility. Details regarding sample preparation, femtosecond transient absorption spectroscopy and global analysis are presented in the Supplementary Material.

Authors' Contributions. All authors designed research; F.M. performed measurements and analyzed data; D.J.K.S. prepared and characterized materials; F.M., M.R.J and R.v.G. wrote the paper.

Competing Interest. We have no competing interest.

Funding. F.M. and R.v.G. were supported by an Advanced Investigator grant from the European Research Council (No. 267333, PHOTPROT) to R.v.G., the TOP-grant (700.58.305) from the Foundation of Chemical Sciences part of NWO and the EU FP7 project PAPETS (GA 323901). R.v.G. gratefully acknowledges his Academy Professor grant from the Netherlands Royal Academy of Sciences. D.J.K.S. and M.R.J. were supported by the Biotechnology and Biological Sciences Research Council of the United Kingdom (project BB/I022570/1).

References

1. Lewis NS, Nocera DG. 2006 Powering the planet: Chemical challenges in solar energy utilization. *Proc. Natl. Acad. Sci. USA* **103**, 15729–15735. (doi: 10.1073/pnas.0603395103)
2. Blankenship RE, Tiede DM, Barber J, Brudvig GW, Fleming GR, Ghirardi M, Gunner MR, Junge W, Kramer DM, Melis A, Moore TA, Moser CC, Nocera DG, Nozik AJ, Ort DR, Parson WW, Prince RC, Sayre RT. 2011 Comparing photosynthetic and photovoltaic efficiencies and recognizing the potential for improvement. *Science* **332**, 805–809. (doi: 10.1126/science.1200165)
3. Inganäs O, Sundström V. 2016 Solar energy for electricity and fuels. *Ambio* **45**, S15–S23. (doi: 10.1007/s13280-015-0729-6)
4. Zhu XG, Long SP, Ort DR. 2008 What is the maximum efficiency with which photosynthesis can convert solar energy into biomass? *Curr. Opin. Biotechnol*. **19**, 153–159. (doi: 10.1016/j.copbio.2008.02.004)
5. Larkum AWD. 2010 Limitations and prospects of natural photosynthesis for bioenergy production. *Curr. Opin. Biotechnol*. **21**, 271–276. (doi: 10.1016/j.copbio.2010.03.004)
6. Zhu XG, Long SP, Ort DR. 2010 Improving photosynthetic efficiency for greater

yield. *Annu. Rev. Plant Biol.* **61**, 235–61. (doi: 10.1146/annurev-arplant-042809-112206)
7. Cotton CAR, Douglass JS, De Causmaecker S, Brinkert K, Cardona T, Fantuzzi A, Rutherford AW, Murray JW. 2015 Photosynthetic constraints on fuel from microbes. *Front. Bioeng. Biotechnol.* **3**, 36. (doi: 10.3389/fbioe.2015.00036)
8. Long SP, Zhu XG, Naidu SL, Ort DR. 2006 Can improvement in photosynthesis increase crop yields? *Plant Cell Environ*. **29**, 315–330. (doi: 10.1111/j.1365-3040.2005.01493.x)
9. Scholes GD, Fleming GR, Olaya-Castro A, van Grondelle R. 2011 Lessons from nature about solar light harvesting. *Nat. Chem*. **3**, 763–774. (doi: 10.1038/nchem.1145)
10. Croce R, van Amerongen H. 2014 Natural strategies for photosynthetic light harvesting. *Nat. Chem. Biol*. **10**, 492–501. (doi: 10.1038/nchembio.1555)
11. Rutherford AW, Osyczka A, Rappaport F. 2012 Back-reactions, short-circuits, leaks and other energy wasteful reactionsin biological electron transfer: Redox tuning to survive life in O_2. *FEBS Lett*. **586**, 603–616. (doi: 10.1016/j.febslet.2011.12.039)
12. Feher G, Allen JP, Okamura MY, Rees DC. 1989 Structure and function of bacterial photosynthetic reaction centers. *Nature* **339**, 111–116. (doi:10.1038/339111a0)
13. Hoff AJ, Deisenhofer J. 1997 Photophysics of photosynthesis. Structure and spectroscopy of reaction centers of purple bacteria. *Phys. Rep.* **287**, 1–247. (doi:10.1016/S0370-1573(97)00004-5)
14. Heathcote P, Jones MR. 2012 The structure-function relationships of photosynthetic reaction centers. In *Comprehensive Biophysics*, Egelman EH, Ferguson S. eds, Academic Press, Oxford, UK, Vol. 8, 115−144.
15. Cogdell RJ, Howard TD, Bittl R, Schlodder E, Geisenheimer I, Lubitz W. 2000 How carotenoids protect bacterial photosynthesis. *Phil. Trans. R. Soc. B* **355**, 1345–1349. (doi: 10.1098/rstb.1978.0090)
16. Ruban AV, Berera R, Ilioaia C, van Stokkum IHM, Kennis JTM, Pascal AA, van Amerongen H, Robert B, Horton P, van Grondelle R. 2007 Identification of a mechanism of photoprotective energy dissipation in higher plants. *Nature* **450**, 575−578. (doi:10.1038/nature06262)
17. Standfuss J, TerwisschavanScheltinga AC, Lamborghini M, Kuehlbrandt W. 2005 Mechanisms of photoprotection and nonphotochemical quenching in pea light-harvesting complex at 2.5 Å resolution. *EMBO J.* **24**, 919−928. (doi:10.1038/sj.10.1038/sj.emboj.7600585)
18. Zinth W, Wachtveitl J. 2005 The first picoseconds in bacterial photosynthesis - ultrafast electron transfer for the efficient conversion of light energy. *ChemPhysChem* **6**, 871–880. (doi: 10.1002/cphc.200400458)
19. Jones MR. 2009 The petite purple photosynthetic powerpack. *Biochem. Soc. Trans.* **37**, 400–407. (doi: 10.1042/BST0370400)
20. Pogorelov TV, Autenrieth F, Roberts E, Luthey-Schulten ZA. 2007 Cytochrome c_2 exit strategy: Dissociation studies and evolutionary implications. *J. Phys. Chem. B* **111**, 618–634. (doi: 10.1021/jp064973i)
21. Van Grondelle R, Bergström H, Sundström V, Gillbro T. 1987 Energy transfer within the bacteriochlorophyll antenna of purple bacteria at 77 K, studied by picosecond absorption recovery. *Biochim. Biophys. Acta.* **894**, 313−326. (doi:10.1016/0005-2728(87)90201-5)
22. Beyer SR, Müller L, Southall J, Cogdell RJ, Ullmann GM, Köhler J. 2015 The

open, the closed, and the empty: time-resolved fluorescence spectroscopy and computational analysis of RC-LH1 complexes from *Rhodopseudomonas palustris*. *J. Phys. Chem. B* **119**, 1362−1373. (doi: 10.1021/jp510822k)
23. Vos MH, Breton J, Martin JL. 1997 Electronic energy transfer within the hexamer cofactor system of bacterial reaction centers. *J. Phys. Chem. B* **101**, 9820−9832. (doi:10.1021/jp971486h)
24. Jordanides XJ, Scholes GD, Fleming GR. 2001 The mechanism of energy transfer in the bacterial photosynthetic reaction center. *J. Phys. Chem. B* **105**, 1652−1669. (doi:10.1021/jp003572e)
25. Breton J, Martin JL, Petrich J, Migus A, Antonetti A. 1986 The absence of a spectroscopically resolved intermediate state P^+B^- in bacterial photosynthesis. *FEBS Lett.* **209**, 37−43. (doi:10.1016/0014-5793(86)81080-8)
26. Jia Y, Jonas DM, Joo T, Nagasawa Y, Lang MJ, Fleming GR. 1995 Observation of ultrafast energy transfer from the accessory bacteriochlorophylls to the special pair in photosynthetic reaction centers. *J. Phys. Chem.* **99**, 6263−6266. (doi: 10.1021/j100017a001)
27. Jackson JA, Lin S, Taguchi AKW, Williams JC, Allen JP, Woodbury NW. 1997 Energy transfer in *Rhodobacter sphaeroides* reaction centers with the initial electron donor oxidized or missing. *J. Phys. Chem. B* **101**, 5747−5754. (doi:10.1021/jp970380j)
28. Vulto SIE, Streltsov AM, Shkuropatov AY, Shuvalov VA, Aartsma TJ. 1997 Subpicosecond excited-state relaxation of the accessory bacteriochlorophylls in native and modified reaction centers of *Rb. sphaeroides* R26. *J. Phys. Chem. B* **101**, 7249−7255. (doi:10.1021/jp963407s)
29. King BA, McAnaney TB, De Winter A, Boxer SG. 2003 Excited-state energy transfer pathways in photosynthetic reaction centers: 5. Oxidized and triplet excited special pairs as energy acceptors. *Chem. Phys.* **294**, 359−369. (doi:10.1016/S0301-0104(03)00318-5)
30. Swainsbury DJK, Scheidelaar S, van Grondelle R, Killian JA, Jones MR. 2014 Bacterial reaction centers purified with styrene maleic acid copolymer retain native membrane functional properties and display enhanced stability. *Angew. Chem. Int. Ed.* **53**, 11803−11807. (doi: 10.1002/anie.201406412)
31. van Brederode ME, van Mourik F, van Stokkum IHM, Jones MR, van Grondelle R.1999 Multiple pathways for ultrafast transduction of light energy in the photosynthetic reaction center of *Rhodobacter sphaeroides*. *Proc. Natl. Acad. Sci. USA* **96**, 2054−2059. (doi: 10.1073/pnas.96.5.2054)
32. van Brederode ME, Jones MR, van Mourik F, van Stokkum IHM, van Grondelle R. 1997 A new pathway for transmembrane electron transfer in photosynthetic reaction centers of *Rhodobacter sphaeroides* not involving the excited special pair. *Biochemistry* **36**, 6855−6861. (doi:10.1021/bi9703756)
33. van Brederode ME, van Stokkum IHM, Katilius E, van Mourik F, Jones MR, van Grondelle R. 1999 Primary charge separation routes in the Bchl:Bphe heterodimer reaction centres of *Rhodobacter sphaeroides*. *Biochemistry* **38**, 7545−7555. (doi: 10.1021/bi9829128)
34. Beekman LMP, Visschers RW, Monshouwer R, Heer-Dawson M, Mattioli TA, McGlynn P, Hunter CN, Robert B, van Stokkum IHM, van Grondelle R, Jones, MR. 1995 Time-resolved and steady-state spectroscopic analysis of membrane-bound reaction centers from *Rhodobacter sphaeroides*: Comparisons with detergent-solubilized complexes. *Biochemistry* **34**, 14712−14721. (doi: 10.1021/bi00045a012)

35. Fajer J, Brune DC, Davis MS, Forman A, Spaulding LD. 1975 Primary charge separation in bacterial photosynthesis: Oxidized chlorophylls and reduced pheophytin. *Proc. Natl. Acad. Sci. USA* **72**, 4956−4960. (doi: 10.1073/pnas.72.12.4956)
36. Kakitani Y, Hou A, Miyasako Y, Koyama Y, Nagae H. 2010 Rates of the initial two steps of electron transfer in reaction centers from *Rhodobacter sphaeroides* as determined by singular-value decomposition followed by global fitting. *Chem. Phys. Lett.* **492**, 142−149. (DOI: 10.1016/j.cplett.2010.03.071)
37. Kovalenko SA, Schanz R, Farztdinov VM, Hennig H, Ernsting NP. 2000 Femtosecond relaxation of photoexcited *para*-nitroaniline: Solvation, charge transfer, internal conversion and cooling. *Chem. Phys. Lett.* **323**, 312−322. (doi: 10.1016/S0009-2614(00)00432-2)
38. Pan J, Lin S, Woodbury NW. 2012 Bacteriochlorophyll excited-state quenching pathways in bacterial reaction centers with the primary donor oxidized. *J. Phys. Chem. B* **116**, 2014−2022. (doi: 10.1021/jp212441b)
39. Jordanides XJ, Scholes GD, Shapley WA, Reimers JR, Fleming GR. 2004 Electronic couplings and energy transfer dynamics in the oxidized primary electron donor of the bacterial reaction center. *J. Phys. Chem. B* **108**, 1753−1765. (doi:10.1021/jp036516x)
40. Kadashchuk A, Vakhnin A, Blonski I, Beljonne D, Shuai Z, Brédas JL, Arkhipov VI, Heremans P, Emelianova EV, Bässler H. 2004 Singlet-triplet splitting of geminate electron-hole pairs in conjugated polymers. *Phys. Rev. Lett.* **93**, 066803. (doi: 10.1103/PhysRevLett.93.066803)
41. Difley S, Beljonne D, Van Voorhis T. 2008 On the singlet-triplet splitting of geminate electron-hole pairs in organic semiconductors. *J. Am. Chem. Soc.* **130**, 3420−3427. (doi: 10.1021/ja0761125)
42. Kadashchuk A, Skryshevski Y, Vakhnin A, Toliautas S, Sulskus J, Augulis R,Gulbinas V, Nespurek S, Genoe J, Valkunas L. 2014 Highly efficient intrinsic phosphorescence from a *σ*-conjugated poly(silylene) polymer. *J. Phys. Chem. C* **118**, 22923−22934. (doi: 10.1021/jp506959)
43. Ma F, Jarenmark M, Hedström S, Persson P, Nordlander E, Yartsev A. 2016 Ultrafast excited state dynamics of $[Cr(CO)_4(bpy)]$: revealing the relaxation between triplet charge-transfer states. *RSC Adv*. **6**, 20507–20515. (doi: 10.1039/c5ra25670d)
44. Williams JC, Alden RG, Murchison HA, Peloquin JM, Woodbury NW, Allen JP. 1992 Effects of mutations near the bacteriochlorophylls in reaction centers from *Rhodobacter sphaeroides. Biochemistry* **31**, 11029−11037. (doi:10.1021/bi00160a012)
45. Woodbury NW, Lin S, Lin XM, Peloquin JM, Taguchi AKW, Williams JC, Allen JP. 1995 The role of reaction-center excited-state evolution during charge separation in a *Rhodobacter sphaeroides* mutant with an initial electron-donor midpoint potential 260 mV above wild-type. *Chem. Phys.* **197**, 405−421. (doi:10.1016/0301-0104(95)00170-S)
46. Huang LB, Ponomarenko N, Wiederrencht GP, Tiede DM. 2012 Cofactor-specific photochemical function resolved by ultrafast spectroscopy in photosynthetic reaction center crystals. *Proc. Natl. Acad. Sci. USA* **109**, 4851−4856. (doi: 10.1073/pnas.1116862109)
47. Richardson DJ, King GF, Kelly DJ, McEwan AG, Ferguson SJ, Jackson JB. 1988 The role of auxiliary oxidants in maintaining redox balance during phototrophic growth of *Rhodobacter capsulatus* on propionate or butyrate. *Arch. Microbiol.*

150, 131−137. (doi: 10.1007/BF00425152)

48. Jones MR, Richardson DJ, McEwan AG, Ferguson SJ, Jackson JB. 1990 In vivo redox poising of the cyclic electron transport system of *Rhodobacter capsulatus* and the effects of the auxiliary oxidants, nitrate, nitrous oxide and trimethylamine *N*-oxide, as revealed by multiple short flash excitation. *Biochim. Biophys. Acta* **1017**, 209−216. (doi:10.1016/0005-2728(90)90186-8)

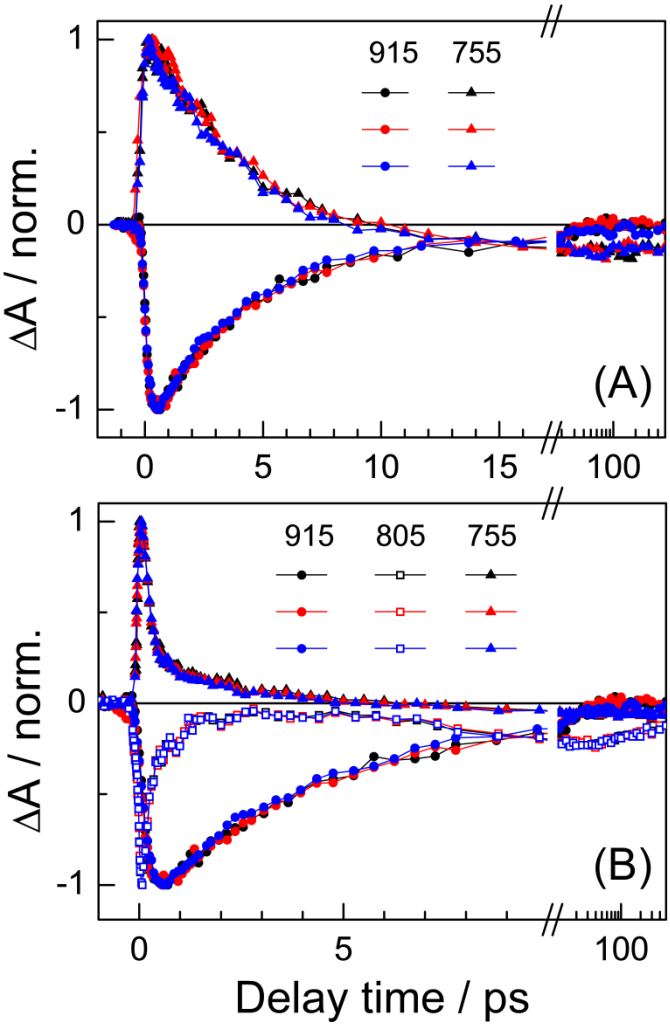

Figure 1. Normalized kinetic traces after excitation of ascorbate-reduced RCs. (A) Excitation of P at 870 nm; (B) Non-selective excitation of B_A/B_B at 805 nm. Traces are for DDM (black), SMA (red) and MEM (blue) RCs at the indicated wavelengths.

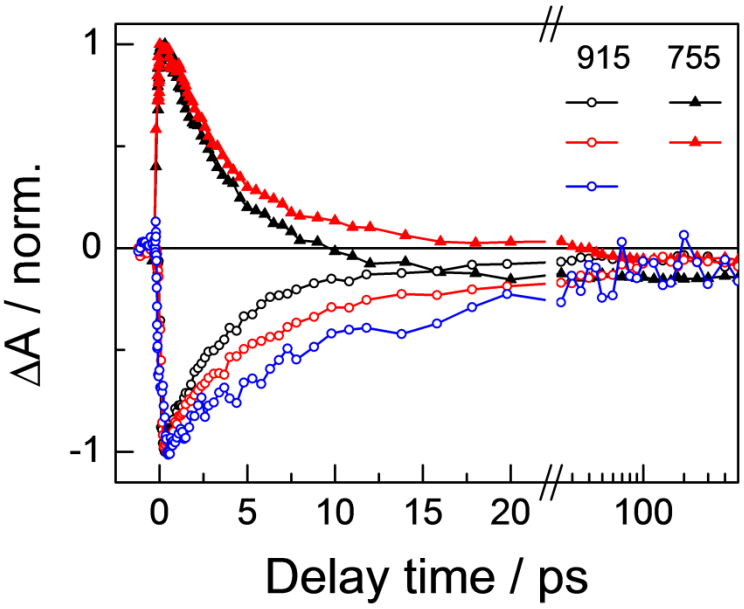

Figure 2. Normalized kinetic traces after excitation of "as-prepared" RCs at 870 nm. Traces are for DDM (black), SMA (red) and MEM (blue) RCs at the indicated wavelengths. The 755 nm kinetic trace for MEM RCs is not shown due to a low signal to noise ratio.

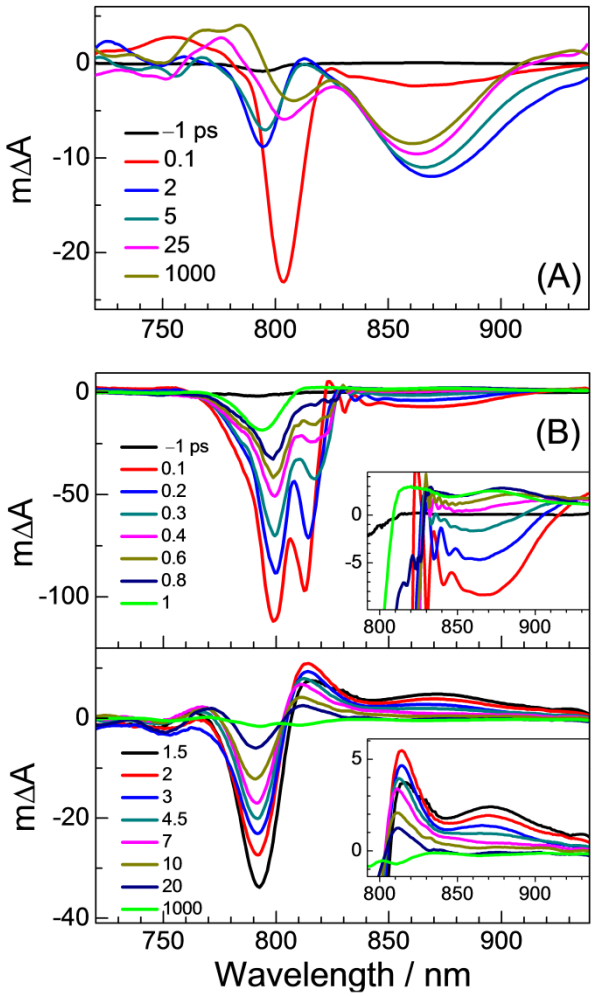

Figure 3. Transient absorption difference spectra after excitation of "as-prepared" RCs at 805 nm. Spectral evolution of DDM (A) and MEM (B) RCs. The insets in (B) show the P-band region on an expanded scale.

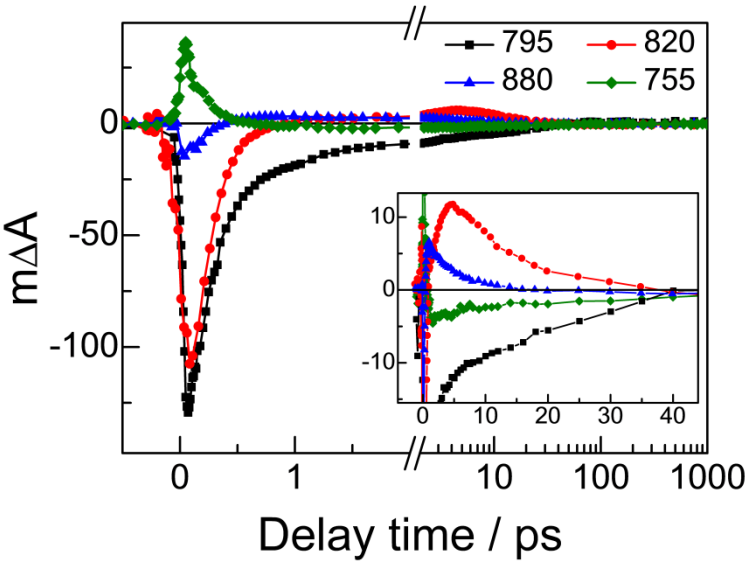

Figure 4. Kinetic traces after excitation of "as-prepared" MEM RCs at 805 nm. The insets show the first 45 ps on an expanded scale.

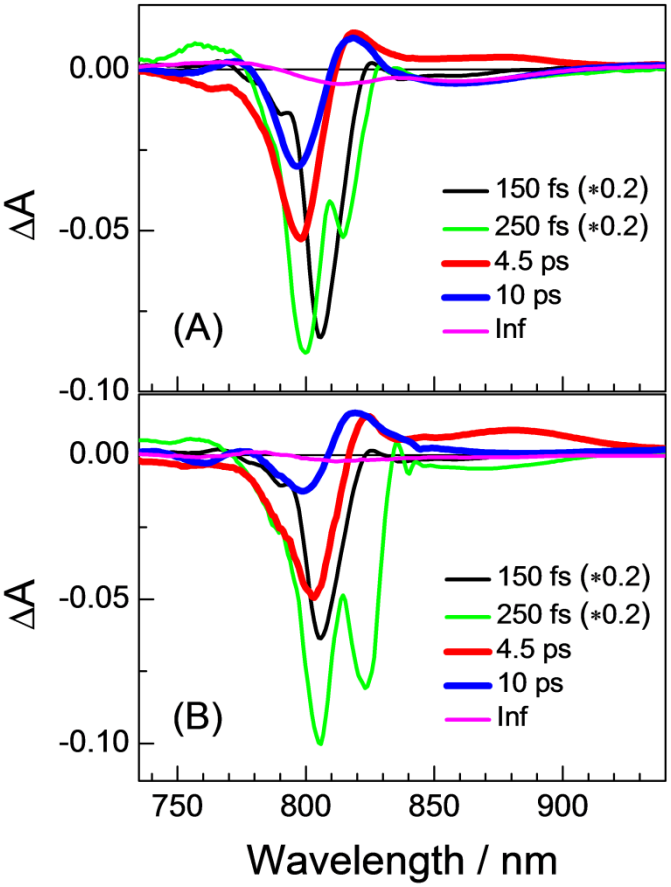

Figure 5. EADS for "as prepared" SMA (A) and MEM (B) RCs after 805 nm excitation.

Scheme 1. Possible fates of B* following excitation of partially oxidized or fully reduced RCs at 805 nm.

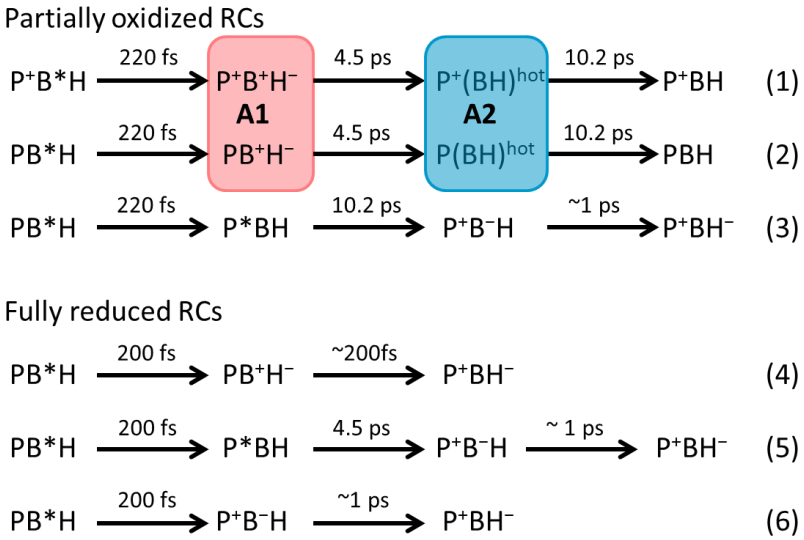

Supplementary Material

Photoprotection through ultrafast charge recombination in photochemical reaction centers under oxidizing conditions

Fei Ma[1,*], David J. K. Swainsbury[2,3], Michael R. Jones[2], and Rienk van Grondelle[1]

[1]Department of Biophysics, Faculty of Sciences, VU University Amsterdam, De Boelelaan 1081, 1081 HV Amsterdam, The Netherlands

[2]School of Biochemistry, University of Bristol, Medical Sciences Building, University Walk, Bristol BS8 1TD, United Kingdom

[3]Present address: Department of Molecular Biology and Biotechnology, University of Sheffield, Sheffield S10 2TN, United Kingdom

Materials and Methods

Sample preparation. Antenna-deficient membranes, RCs purified with *n*-dodecyl *β*-D-maltoside (DDM) and RCs purified with SMA were prepared as described previously [30]. Membranes were suspended in 20 Mm Tris (pH 8.0), and for SMA and DDM RCs this buffer was supplemented with 6% (w/v) SMA or 0.04% (w/v) DDM, respectively. For fully-reduced conditions 20 mM sodium ascorbate and 200 μM phenazinemetho sulfate (PMS) were added.

Femtosecond transient absorption spectroscopy. A tunable optical parametric amplifier (OPA, Coherent OperA) pumped by a Ti:sapphire-based amplified laser (Coherent Legend, 800 nm) were used to produce pump pulses. The probe pulse was generated by focusing a small fraction of the 800 nm pulse into a sapphire plate. The pump pulse was centered at 870 nm or 805 nm with 10 nm full width at half

maximum (FWHM). The overall temporal resolution was ~120 fs. Transient absorption experiments were performed under magic angle polarization conditions and at room temperature. The sample absorbance was kept at OD_{870} = ~0.2 and OD_{805} = ~0.5, in a 0.2 mm cell. The excitation energy was 100 nJ per pulse, and was in the linear excitation region. The sample cell was moving during measurements to avoid the accumulation of long-lived species. After each measurement, the absorbance of P at 870 nm decreased by less than 1%. For global analysis, datasets were analyzed simultaneously with linked kinetics and an instrument response function using an irreversible sequential model with up to five increasing lifetimes.

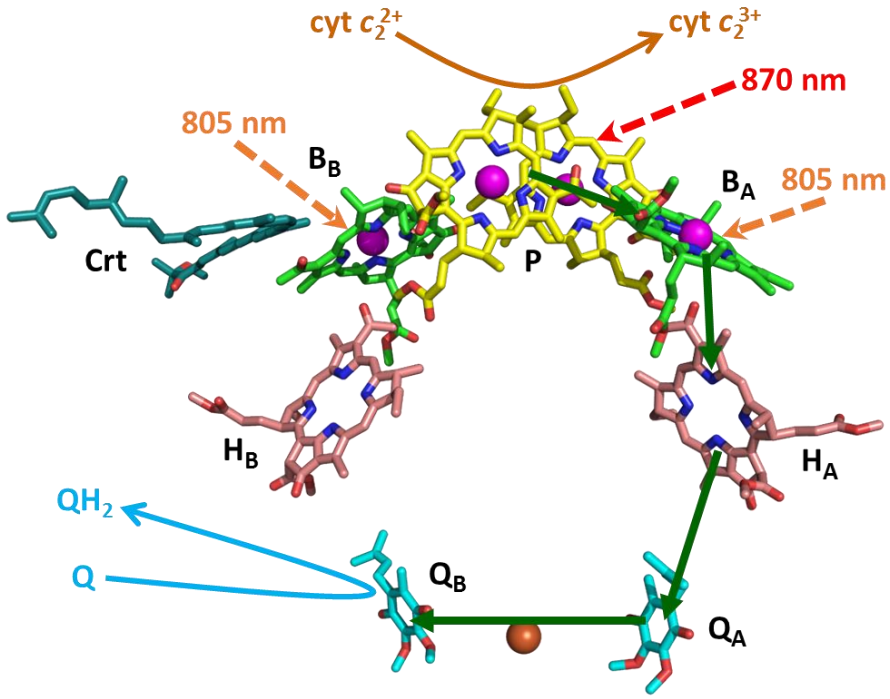

Figure S1. Arrangement of cofactors in the *Rba. sphaeroides* RC and interactions with diffusible electron carriers. Membrane-spanning charge separation is facilitated by a pair of excitonically-coupled BChls (P), a monomeric BChl (B_A), a BPhe (H_A) and a ubiquinone (Q_A). The terminal acceptor is a ubiquinone (Q_B) which binds to the RC in the oxidized form (Q) and dissociates in the doubly reduced/doubly protonated form (Q_BH_2) (cyan arrow), transferring electrons to the cyt bc_1 complex in a few milliseconds [S1]. The P^+ created by charge separation is re-reduced by a cyt c_2 which binds to the periplasmic face of the RC (brown arrow). The reaction cyt $c_2^{2+}P^+ \rightarrow$cyt $c_2^{3+}P$ occurs on a timescale of microseconds to milliseconds depending on the redox state of the cyt c_2 pool [21]. The B_B and H_B cofactors do not participate in membrane-spanning electron transfer and so despite apparent structural symmetry this RC displays a strong functional asymmetry with "active" and "inactive" cofactor branches. The B_B BChl is involved in singlet energy transfer from the carotenoid (Crt) to P [S2], triplet energy transfer from P to the carotenoid [S3,S4], and its presence maintains (pseudo)symmetrical environment for the P dimer. The question of why H_B is a specialized BPhe cofactor, and why it is present at all, remains unresolved (see [14,19,S5] for discussions). The principal function of the carotenoid is quenching of the energy of long-lived BChl triplet excited states [15]. In addition the primary electron donor cation P^+ is able to quench excited state energy donated either by the LH1 antenna BChls [21,21] or by the monomeric BChls and BPhes of the RC [25−29].

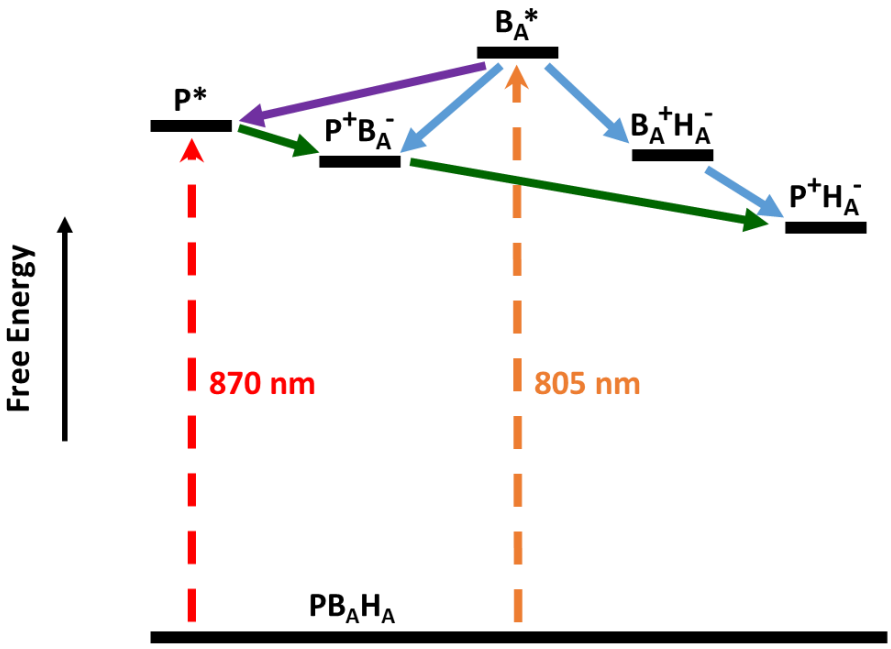

Figure S2. Schematic of mechanisms of charge separation in the *Rba. sphaeroides* RC. Excitation of P into its first singlet excited state (P*) shunts the potential for oxidation of the P BChls to a much more negative value; experimentally this can be achieved by excitation into the P-band at 870 nm (red dashed arrow). Creation of P* triggers formation of the radical pair $P^+B_A^-$ with a time constant of 3-5 ps, followed by formation of $P^+H_A^-$ with a time constant of 0.5-2 ps (green arrows) (for reviews see [12,13,14,18,19]). Further stabilization of this radical pair occurs through electron transfer to Q_A and Q_B (not shown). If B_B, H_A, H_B (not shown) or B_A are excited directly (orange dashed arrow), excited state energy is transferred to P within a few hundred femtoseconds (purple arrow) [23−29]. In parallel, excitation of B_A results in direct sub-picosecond formation of $P_A^+B_A^-$ and/or $B_A^+H_A^-$, both of which relax to $P^+H_A^-$ with a time constant of 1-2 ps (blue arrows) [31−33,42]. Studies with wild-type and mutated RCs indicate that a fine balance exists between the yields of these three possible decay routes for B_A*. In wild-type RCs a 50:50 ratio of B_A* decay via P* and $P^+B_A^-$ was proposed [31], and subsequently confirmed in crystals of WT RCs [42]. In a mutated YM210W RC, where the rate of P*→$P^+B_A^-$ is strongly slowed, it was estimated that B* decayed 57 % by energy transfer to P, 29 % by direct formation of $P^+B_A^-$ and 14 % by direct formation of $B_A^+H_A^-$ [32], each decay process proceeding with a similar lifetime. In a RC with a heterodimer BChl:BPhe primary donor (D) it was proposed that 60 % of B* decayed via D* and 40 % via B^+H^- [33], and in a YM210L mutated RC this B^+H^- route was also prominent [S6].

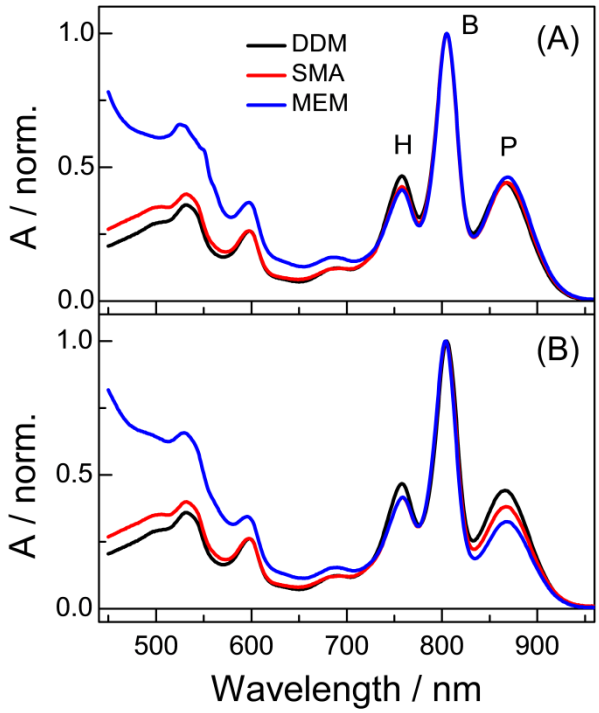

Figure S3. Normalized steady-state absorption spectra of DDM-purified, SMA-purified and membrane-embedded (MEM) RCs. (A) RCs incubated with 20 mM ascorbate and 200 μM PMS. (B) "As-prepared" RCs without added ascorbate. During purification in oxygenated buffers, SMA and MEM RCs show partial oxidation of the P BChls, manifested as a partial bleaching of the relevant P-band at 865 nm.

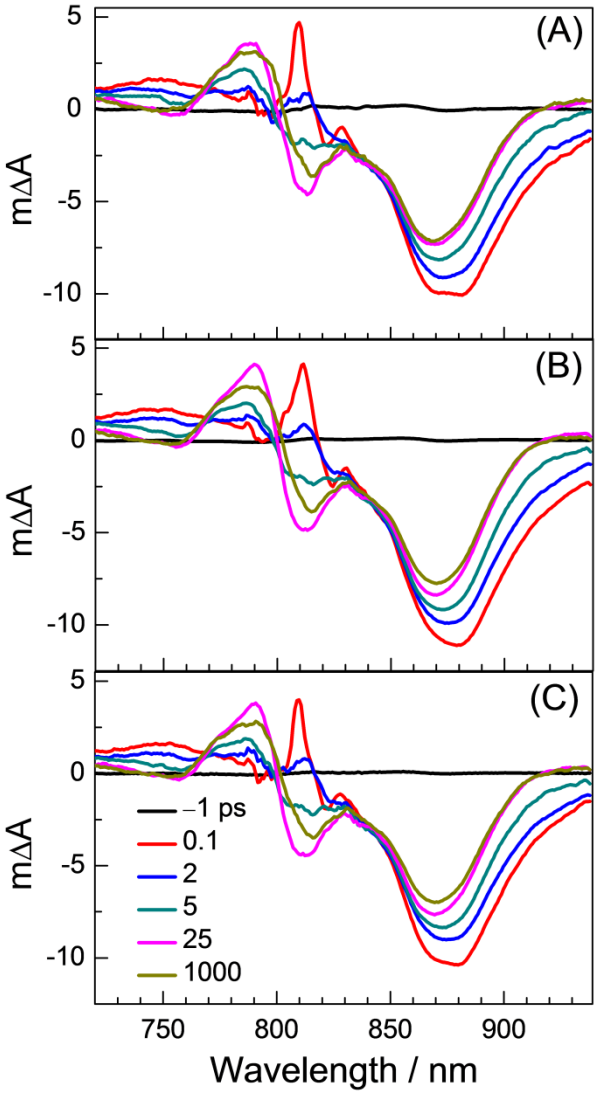

Figure S4. Transient absorption difference spectra after excitation of ascorbate-reduced RCs at 870 nm. Spectral evolution of DDM (A), SMA (B) and MEM (C) RCs.

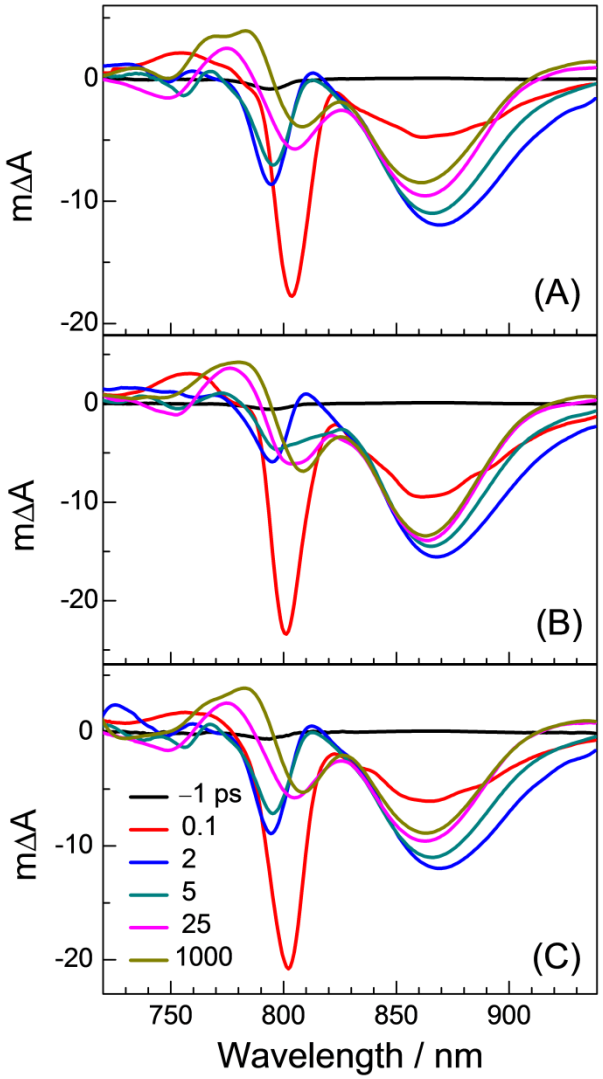

Figure S5. Transient absorption difference spectra after excitation of ascorbate-reduced RCs at 805 nm. Spectral evolution of DDM (A), SMA (B) and MEM (C) RCs.

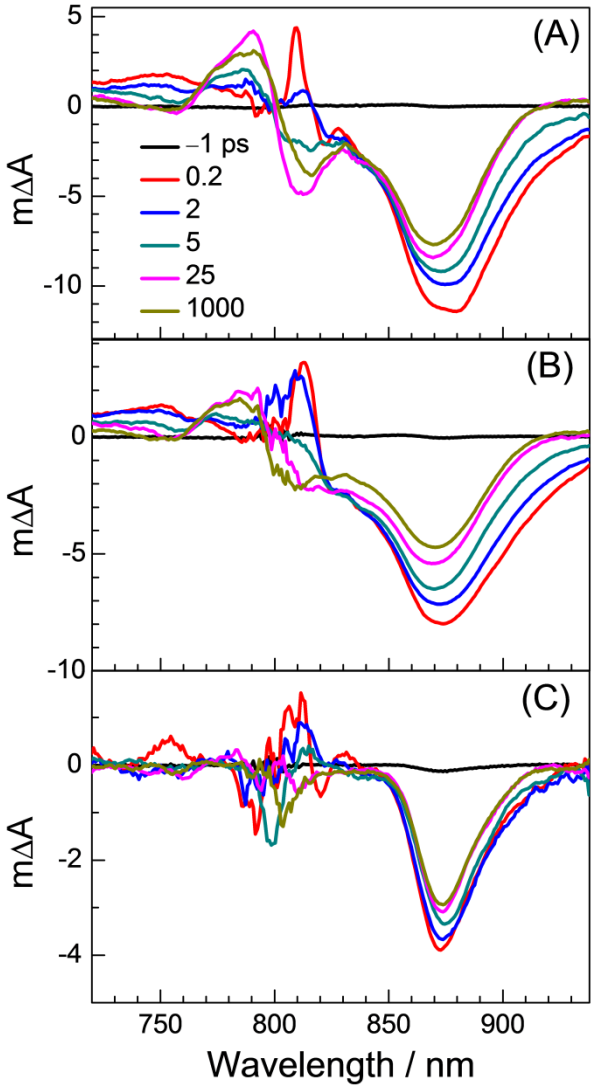

Figure S6. Transient absorption difference spectra after excitation of "as-prepared" RCs at 870 nm. Spectral evolution of DDM (A), SMA (B) and MEM (C) RCs.

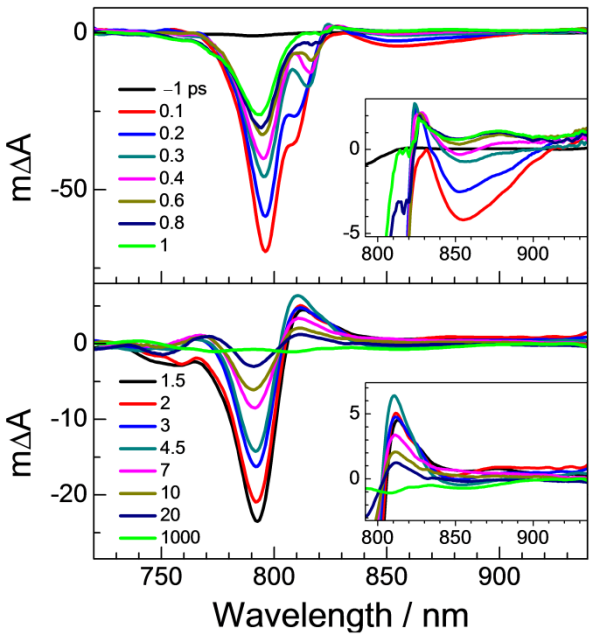

Figure S7. Transient absorption difference spectra after excitation of "as-prepared" SMA RCs at 805 nm.

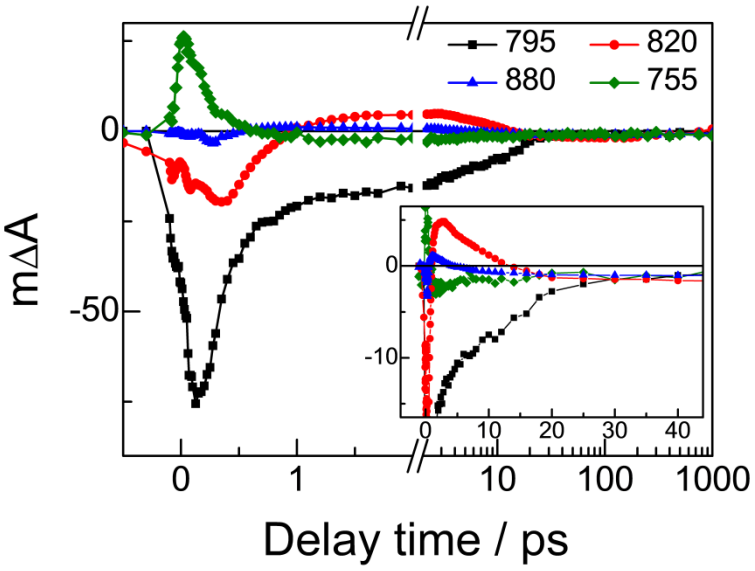

Figure S8. Kinetic traces after excitation of "as-prepared" SMA RCs at 805 nm. The insets show the first 45 ps on an expanded scale.

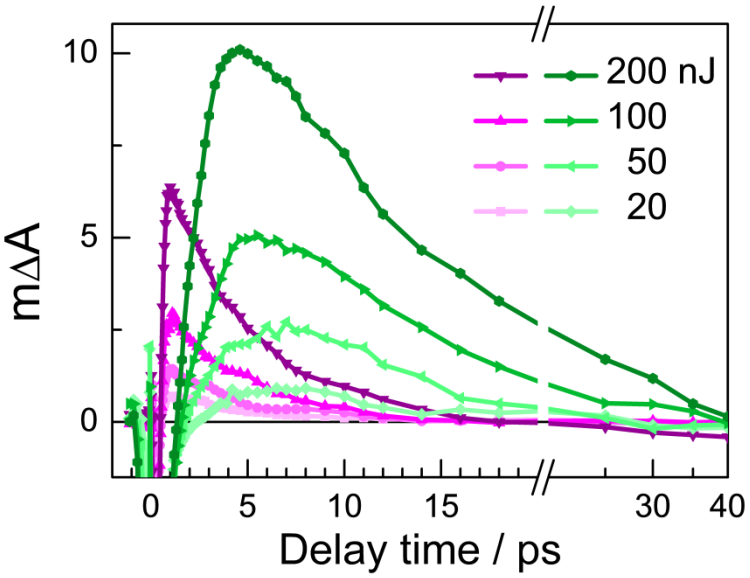

Figure S9. Linear dependence of kinetic traces after excitation of MEM RCs at 805 nm on excitation energy. The detection wavelength is 880 nm (violet) and 820 nm (green) under the indicated energies.

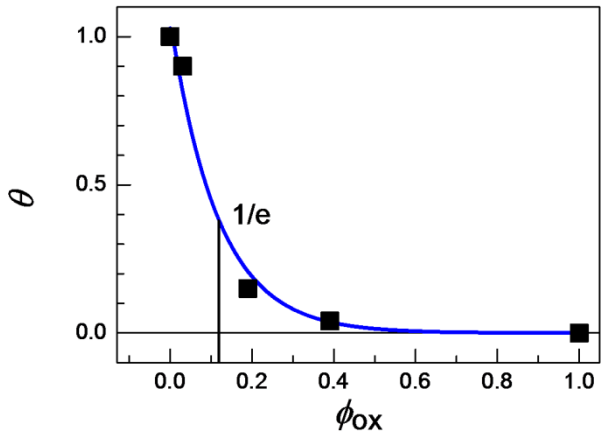

Figure S10. Dependence of the $P^{+}Q_{A}^{-}$ formation (θ) on the oxidation ratio ($\emptyset_{ox}$), and the exponential fitting curve.

References

S1. Comayras F, Jungas C, Lavergne J. 2005 Functional consequences of the organization of the photosynthetic apparatus in *Rhodobacter sphaeroides* - II. A study of PufX(-) membranes. *J. Biol. Chem.* **280**, 11214−11223. (doi: 10.1074/jbc.M412089200)

S2. Lin S, Katilius E, Ilagan RP, Gibson GN, Frank HA, Woodbury NW. 2006 Mechanism of carotenoid singlet excited state energy transfer inmodified bacterial reaction centers. *J. Phys. Chem. B* **110**, 15556–15563. (doi: 10.1021/jp992259d)

S3. Frank HA, Violette CA. 1989 Monomeric bacteriochlorophyll is required for the triplet energy-transfer between the primary donor and the carotenoid in photosynthetic bacterial reaction centers. *Biochim. Biophys. Acta*.**976**, 222−232. (doi:10.1016/S0005-2728(89)80234-8)

S4. deWinter A, Boxer SG. 1999 The mechanism of triplet energy transfer from the special pair to the carotenoid in bacterial photosynthetic reaction centers. *J. Phys. Chem. B* **103**, 8786−8789. (doi**:** 10.1021/jp992259d)

S5. Watson AJ, Fyfe PK, Frolov D, Wakeham, MC, Nabedryk E, van Grondelle R, Breton J, Jones MR. 2005 Replacement or exclusion of the B-branch bacteriopheophytin in the purple bacterial reaction centre: the H_B cofactor is not required for assembly or core function of the *Rhodobacter sphaeroides* complex. *Biochim. Biophys. Acta*. **1710**, 34−46. (doi: 10.1016/j.bbabio.2005.08.005)

S6. van Brederode ME, Ridge JP, van Stokkum IHM, van Mourik F, Jones MR, van Grondelle R. 1998 On the efficiency of energy transfer and the different pathways of electron transfer in mutant reaction centers of *Rhodobacter sphaeroides*. *Photosynth. Res.* **55**, 141−146. (doi: 10.1023/A:1005925917867)